Journal of Atmospheric and Solar-Terrestrial Physics 72 (2010) 1139–1146

Contents lists available at ScienceDirect

Journal of Atmospheric and Solar-Terrestrial Physics

journal homepage: www.elsevier.com/locate/jastp

Short Communication

First results of warm mesospheric temperature over Gadanki (13.5°N, 79.2°E) during the sudden stratospheric warming of 2009

S. Sridharan [a,*], K. Raghunath [a], S. Sathishkumar [b], D. Nath [a]

[a] National Atmospheric Research Laboratory, Gadanki, India
[b] Equatorial Geophysical Research Laboratory, Indian Institute of Geomagnetism, Tirunelveli, India

ARTICLE INFO

Article history:
Received 5 February 2010
Received in revised form
4 June 2010
Accepted 7 June 2010
Available online 15 June 2010

Keywords:
Major sudden stratospheric warming
Gravity waves
Planetary waves
Meridional circulation

ABSTRACT

Rayleigh lidar observations at Gadanki (13.5°N, 79.2°E) show an enhancement of the nightly mean temperature by 10–15 K at altitudes 70–80 km and of gravity wave potential energy at 60–70 km during the 2009 major stratospheric warming event. An enhanced quasi-16-day wave activity is observed at 50–70 km in the wavelet spectrum of TIMED–SABER temperatures, possibly due to the absence of a critical level in the low-latitude stratosphere because of less westward winds caused by this warming event. The observed low-latitude mesospheric warming could be due to wave breaking, as waves are damped at 80 km.

1. Introduction

A sudden stratospheric warming (SSW) event is a dramatic event in the winter middle atmosphere that involves profound changes of temperature and wind circulation in a short period of time (Scherhag, 1952; Andrews et al., 1987). The principal mechanism behind the formation of this event is the interaction of upward propagating planetary waves with the transient wave and mean flow (Matsuno, 1971). The wave mean flow interaction decelerates and even reverses the eastward winter stratospheric jet. The meridional circulation associated with the SSW can induce upwelling in the tropics and produce cooling in the equatorial lower stratosphere. The association of cooling in the tropical latitudes was first observed by Fritz and Soules (1970) in NIMBUS satellite observations. Mukherjee and Ramana Murty (1972) noticed occasional warming occurring at tropical latitudes over India in the upper stratosphere and mesosphere. Later Sridharan et al. (2009) observed a warm stratopause in Rayleigh lidar temperature observations over Gadanki (13.5°N, 79.2°E), coinciding with high latitude stratopause cooling, associated with the end of a major SSW event in 2006. The authors suggested based on Matsuno (1971) that it could be due to ascending (descending) motions at high (low) latitudes above the critical level of planetary waves, where there was no planetary wave flux. Shepherd et al. (2007) also observed mesospheric cooling at a time of stratospheric warming in the tropics correlated with SSW events at mid- and high latitudes.

Accompanying the SSW, the Matsuno's (1971) modeling study showed cooling in the high latitude mesosphere, which was confirmed by a number of observational studies (Gregory and Manson, 1975; Whiteway and Carswell, 1994). In the Holton (1983) numerical modeling study, which applied parameterization of gravity wave saturation effects, a SSW event was accompanied by a mesospheric cooling due to radiative processes. Dunkerton and Butchart (1984) performed a ray-tracing study of gravity wave propagation through a SSW and observed that the presence of large amplitude planetary waves leads to propagating and forbidden zones, which reduce, but not eliminate, gravity wave propagation into the mesosphere. However, recent model results show that the deceleration/reversal of eastward polar jet allows more eastward propagating gravity waves to propagate into the mesosphere, forcing an equatorward and upward meridional circulation, which can cause polar mesospheric cooling (Liu and Roble, 2002).

No previous observational studies have focused specifically on the effect of SSW events on low-latitude mesospheric thermal structure and gravity wave propagation. In this study, for the first time, we report on low-latitude Rayleigh lidar observations of temperature structure and planetary and gravity wave activities over a time period prior to and during the occurrence of a major SSW during the end of January 2009. Our Rayleigh lidar provides routine observations of the temperature structure in the upper stratosphere and mesosphere with a vertical and temporal resolution that cannot be obtained with satellite or rocket techniques.

* Corresponding author. Tel.: +91 8585 272124; fax: +91 8585 272018.
E-mail address: susridharan@narl.gov.in (S. Sridharan).

1364-6826/$ - see front matter © 2010 Elsevier Ltd. All rights reserved.
doi:10.1016/j.jastp.2010.06.003

2. Instrumentation, data analysis and results

The state of the high-latitude winter hemisphere during January 2009 is depicted in Fig. 1(a)–(b) using the (UKMO) UK Meteorological Office data set, which is a result of assimilation of in situ and remotely sensed data into a numerical forecast model of the stratosphere and troposphere. A description of the data assimilation system is given by Swinbank and O'Neill (1994). During the beginning of January 2009, normal winter conditions can be observed with poleward decrease in temperature inferred from the negative polar temperature gradient and prevailing eastward winds at polar latitudes. However, a major SSW event occurred during January 21–27, which can be identified from the positive temperature difference between pole and 60°N associated with the reversal of winds at 61°N from eastward to westward at 10 hPa (Labitzke and Naujokat, 2000). According to Manney et al. (2009), the 2009 major SSW event was remarkable and characterized by a splitted polar vortex.

In order to study the change in thermal structure over low-latitudes associated with the spectacular warming event, Rayleigh lidar observations were carried out at Gadanki during January 2009. The lidar system had been using a low power laser source (500 mJ/pulse, 20 Hz pulse repetition frequency (PRF)), which has recently been replaced with a new one, with 600 mJ/pulse with 50 Hz PRF. The laser transmits its second harmonic output at a wavelength of 532 nm vertically upwards and the backscattered photons are collected with a 75 cm diameter Newtonian telescope and are counted sequentially using a multichannel scaling averager, into successive range bins of equivalent width of 300 m. Under the 'Study of Atmospheric Forcing and Response' (SAFAR) program of the National Atmospheric Research Laboratory (NARL; Jayaraman et al., 2009), the Rayleigh lidar observations were carried out for about 5 h during most of the cloud free nights of January 2009, anticipating the high latitude major warming event, which did occur during 21–27 January 2009, to study the influence of the SSW events on the tropical thermal structure. The Rayleigh lidar technique is based on assumption that in the absence of aerosol (i.e. above 30 km altitude), the backscattering photons are directly proportional to molecular density. With the new high power laser, there is a significant improvement in the molecular returns and the standard error in the derivation of temperature, which depends mainly on the number of photon counts, is obtained at heights ~5 km higher than the one obtained with the low power laser. For example, if the standard error is 20 K at 85 km with the low power laser, nearly the same standard error is obtained around 90 km with the

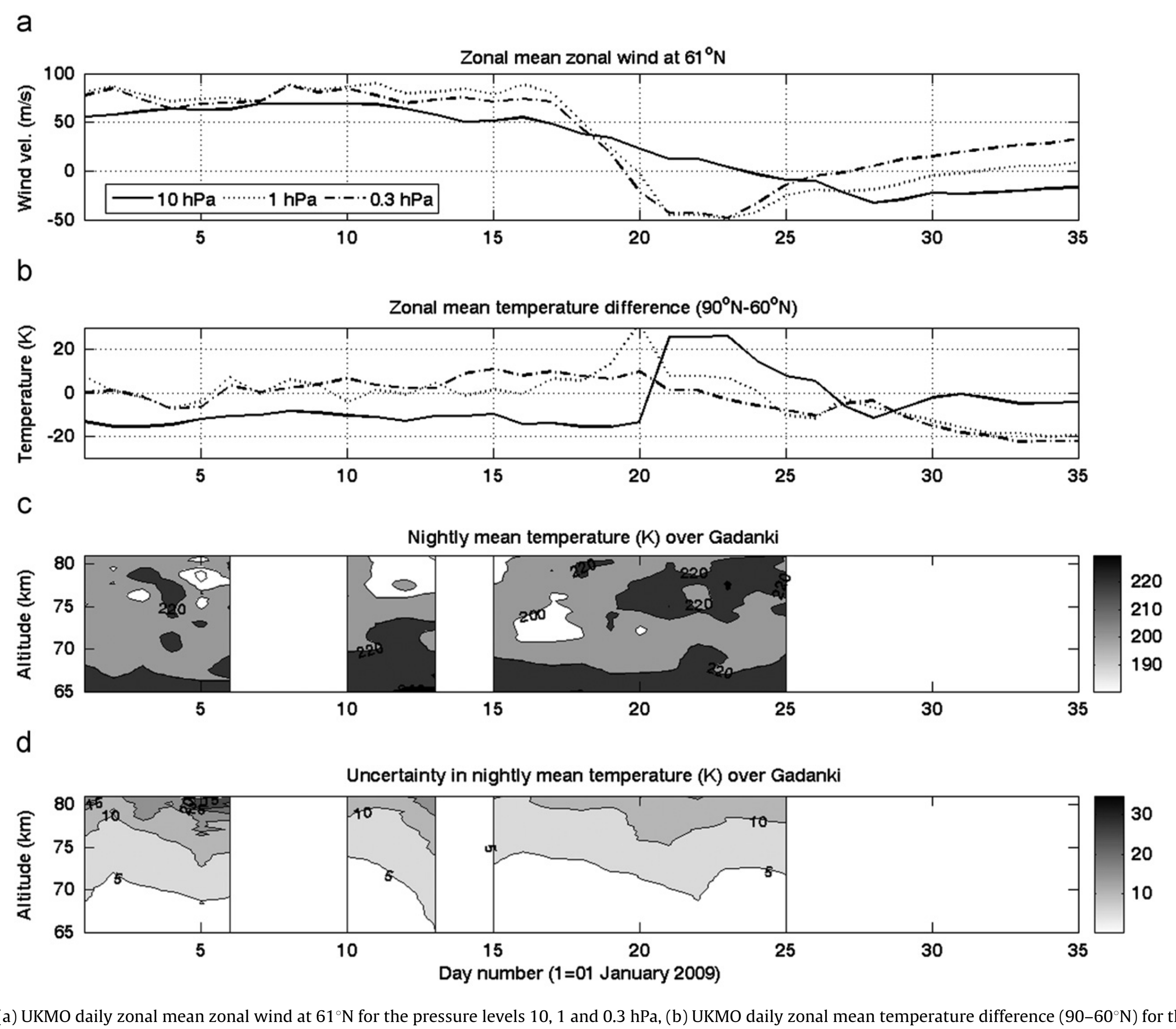

Fig. 1. (a) UKMO daily zonal mean zonal wind at 61°N for the pressure levels 10, 1 and 0.3 hPa, (b) UKMO daily zonal mean temperature difference (90–60°N) for the same pressure levels, (c) Rayleigh lidar nightly mean temperature over Gadanki (13.5°N, 79.2°E) and (d) its uncertainty for the altitudes 65–81 km. The white blocks in (c) and (d) denote data gaps.

high power laser. Though we took much effort to operate the lidar for about 5 h with 30 s time resolution on each cloud free night, there are a few data gaps on the days 7–9, 14 and 26 January 2009. After 29 January 2009, we could not operate the lidar due to system problems and the operation resumed only on 6 February 2009. Using half-an hour integrated photon counts profiles, a relative density profile is obtained by correcting for range-squared dependence and normalizing the backscatter profile at an altitude of 40 km. From relative density profiles, pressure profiles are derived by seeding with the CIRA-86 model pressure at the top reference height of 90 km and performing downward integration using the hydrostatic equation and then from the pressure profile, an absolute temperature profile in the altitude region 30–90 km is derived using the ideal gas equation (Hauchecorne and Chanin, 1980; Siva Kumar et al., 2003). These half an hour temperature profiles are used for estimating gravity wave potential energy per unit mass. However, in order to obtain nightly mean temperature profile with less uncertainty, the photon counts integrated for four and half hours (to maintain uniformity for all the nights) are used. The nightly averaged temperature, so computed, for the altitudes 65–80 km over Gadanki and their uncertainty are shown in Fig. 1(c) and (d), respectively. It can be observed that the nightly mean temperature is larger in the altitude region 70–80 km on days 20–25 January 2009, when compared with the rest of the observation period. The temperature increases from ~185 K on day 12, reaches a maximum of ~250 K on day 23 and decreases to 193 K on day 29. The nightly mean temperature averaged prior (15–20 January 2009) and during (21–25 January 2009) warming are averaged and plotted in Fig. 2 for comparison. The TIMED–SABER temperature profiles averaged daily for the latitudes 10–15°N and longitudes 60–90°E are used to confirm the warming event observed by the lidar. The (SABER) sounding of atmosphere by broadband emission radiometry can be briefly described as a 10-channel broad-band limb viewing, infrared radiometer that has been measuring stratospheric and mesospheric temperatures, mainly from the 15 μm emission of CO_2, since the launch of the Thermosphere, Ionosphere, Mesosphere Energetics and Dynamics (TIMED) satellite. The data retrieval method and their validation are described in Remsberg et al. (2003). There are a few studies that made comparisons with Rayleigh lidar temperature over Gadanki with SABER temperatures (Guharay et al., 2009 for example). It can be observed that there is an enhancement in temperature in the altitude region ~70–80 km in both Rayleigh lidar and SABER temperature profiles. The lidar temperature averaged for days before the warming (15–20 January 2009) exceeds that during the warming (21–25 January 2009) by 5–7 K at altitudes 55–63 km and the latter exceeds the former by 10–15 K at altitudes 70–78 km. In the case of SABER temperature, the temperature profiles averaged before the warming exceed those during the warming by ~5 K at slightly lower altitude of 58–60 km. The temperature profile after the warming exceeds the one before the warming by 10–15 K in the lower altitude region 68–74 km. As the estimated accuracy of SABER temperatures is 1.5 K at altitudes 15–80 km and 4 K above 80 km, the SABER temperature profiles also confirm the mesospheric warming event (Mertens et al., 2004).

We also investigated, whether there is an enhancement in gravity wave activity prior and during the warming. Gravity wave activity has been observed in profiles of relative temperature perturbations $T''(z)/T_o(z)$. Perturbation profiles $T''(z)$ are extracted by subtracting each 30 min averaged profiles from the nightly mean temperature profile, smoothed by 3 km in altitude. The mean squared relative fluctuations as a function of altitude is calculated by averaging $(T''(z)/T_o(z))^2$. From this we determine the profile of RMS perturbations and then subtracting noise variance due to statistical uncertainty at each altitude. The average potential energy per unit mass is calculated from

$$E_p(z) = \frac{1}{2}(g/N(z))^2(\overline{T'(z)}/T_o(z))^2$$

The Brunt–Väisälä frequency squared, N^2, is calculated by differentiating the mean temperature profile over adjacent three heights (Tsuda et al., 2000). Typical values of the error in E_p is less than 20% below 70 km. However, above 70 km altitude, the error increases drastically to 60% at 80 km and hence E_p values are presented only upto ~70 km.

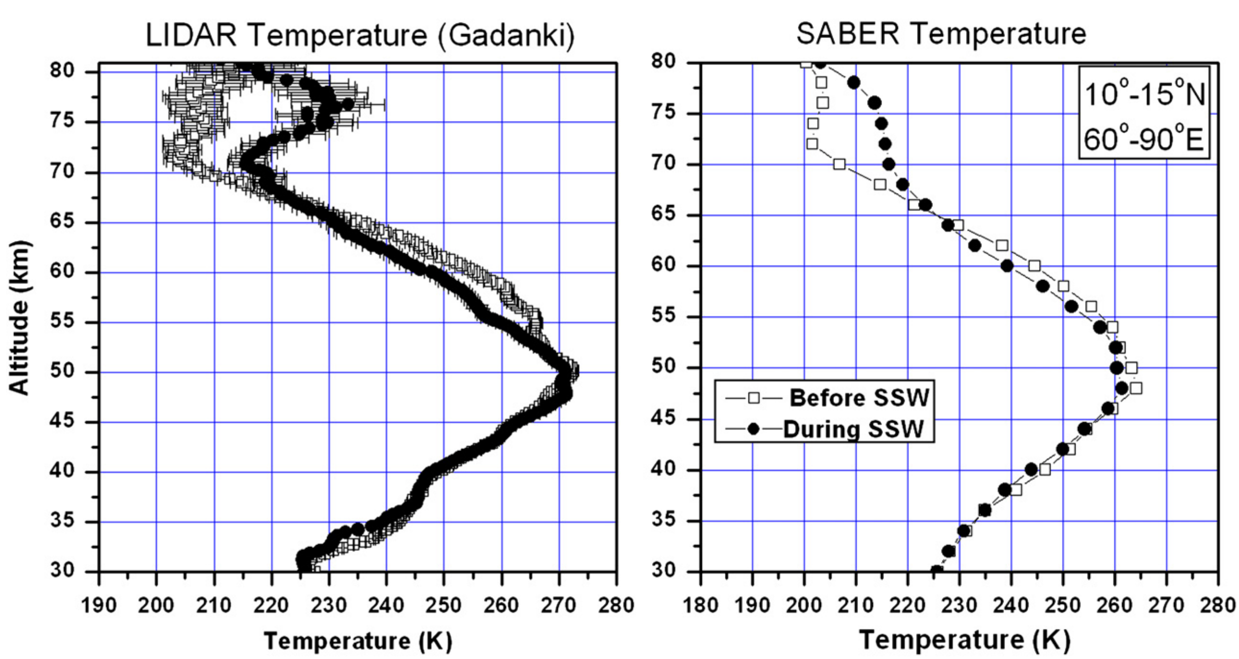

Fig. 2. Altitude profile of Rayleigh lidar temperature over Gadanki (left panel) and TIMED–SABER temperature averaged for the latitudes 10–15°N and 60–90°E before (line with square) and during (line with circle) the 2009 SSW event.

From the time-altitude cross section of nightly potential energy per unit mass, shown in Fig. 3, we can infer that E_p values are larger on days 20–23 January 2009 corresponding to the onset of the SSW event. In particular, at 65 km, E_p values are observed to be two times larger during the warming event than before. E_p values are near ~50 J/kg during 1–6 January 2009 and they increase to nearly ~100 J/kg during 18–21 January 2009. The large enhancement of gravity potential energy appears to be related to the large enhancement in polar stratospheric temperature (top panel). The large enhancement of E_p can also be observed even during 11–12 January 2009. It may be noted that enhancement in polar stratospheric temperature occurs at 0.3 hPa a few days earlier and propagates downward.

In order to see whether there is any planetary wave activity during the winter, the daily TIMED-SABER temperatures averaged for latitudes 10–15°N and longitudes 60–90°E for the winter period November 2008–March 2009 are subjected to wavelet analysis. For analyzing localized variations of power within a time series, the wavelet analysis is the best choice, when compared to other frequently used short-term Fourier analysis method. By decomposing a time series into time–frequency space, it is possible to determine both the dominant modes of variability and how those modes vary in time (Daubechies, 1992). For the present study, we use a Morlet wavelet function as the mother wavelet. The Morlet wavelet, which is a plane wave modulated by Gaussian, is given by

$$\psi_o(\eta) = \pi^{-1/4} e^{i\omega_o \eta} e^{-\eta^2/2}$$

where ω_o is the non-dimensional frequency, taken in the present study to be 6 to satisfy the admissibility condition and η is the non-dimensional time parameter (Torrence and Compo, 1999). The normalized Morlet wavelet spectra of TIMED-SABER temperatures at 50, 66, 72, 76 and 80 km altitudes, averaged for 60–90°E and 10–15°N are shown in Fig. 4 for the period January–February 2009. The 95% confidence level is shown by the thick contours. The cone of influence is plotted as crossed lines in which edge effects are important, as one goes to larger periods. The figure clearly reveals the presence of strong 16-day planetary wave activity prior to and during the SSW event at altitudes 50–70 km, whereas the activity is absent at 80 km. The absence of wave activity at 80 km suggests that the wave breaking might have occurred in the altitude region 70–80 km. We also analyzed the MF radar winds at 88 and 92 km over Tirunelveli and the spectrum of zonal winds shows that the 16-day wave energy is considerably damped during the SSW event (not shown). Observations of 16-day westward planetary waves in the MLT region have frequently been reported (Luo et al., 2002; Lima et al., 2006; Vineeth et al., 2009 to state a few). The altitude profiles of amplitudes and phases of ~16-day westward propagating wave of zonal wavenumber (k) 1 and 2 in SABER temperature is shown in Fig. 5. It can be observed from the figure that the amplitude of wave ($k=2$) is larger than that of wave ($k=1$). The wave ($k=2$) amplitude shows two peaks—one around 55 km (1.5 K) and the other between 70 and 75 km (2.5 K). The wave ($k=1$) also shows maximum amplitude (1.5 K) at altitudes between 70 and 75 km. Both amplitudes decrease drastically around 75 km. The phase of wave ($k=2$) shows downward progression with the vertical wavelength of ~37 km, whereas the phase of wave ($k=1$) does not show clear downward progression.

3. Discussion and conclusion

The nightly averaged Rayleigh lidar observations over Gadanki (13.5°N, 79.2°E) show 10–15 K warmer temperatures in the altitude region 70–80 km during 21–25 January 2009, when there

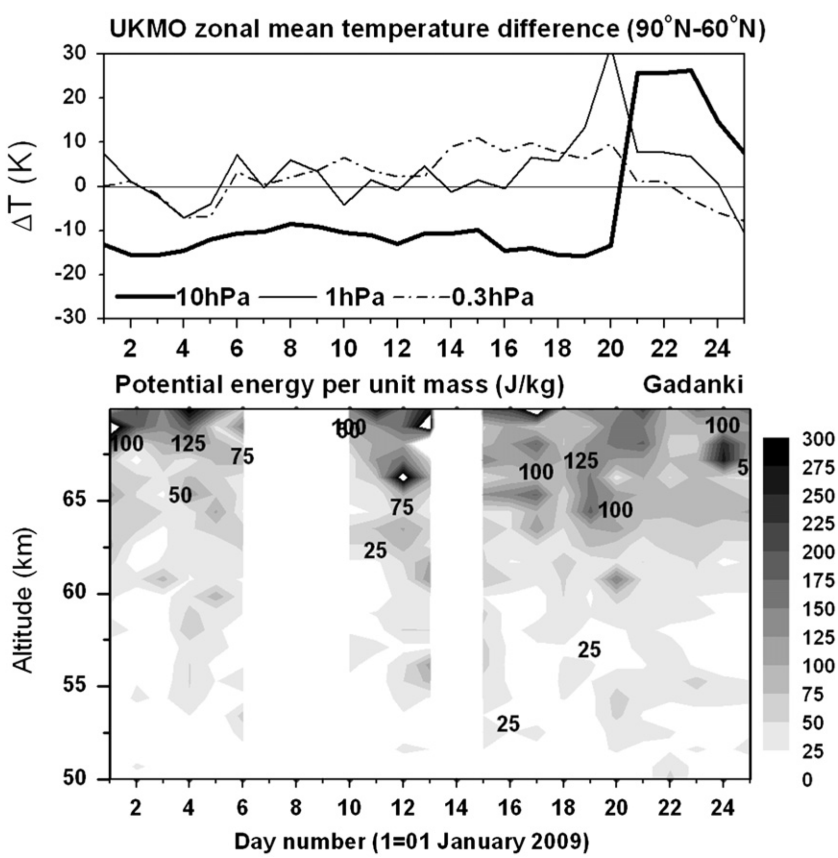

Fig. 3. Potential energy per unit mass for the altitudes 50–70 km estimated from the lidar temperature perturbations over Gadanki (bottom panel) and the UKMO poleward zonal mean temperature differences at 10, 1 and 0.3 hPa (top panel) to identify the thermal state of high latitude winter for 01–25 January 2009.

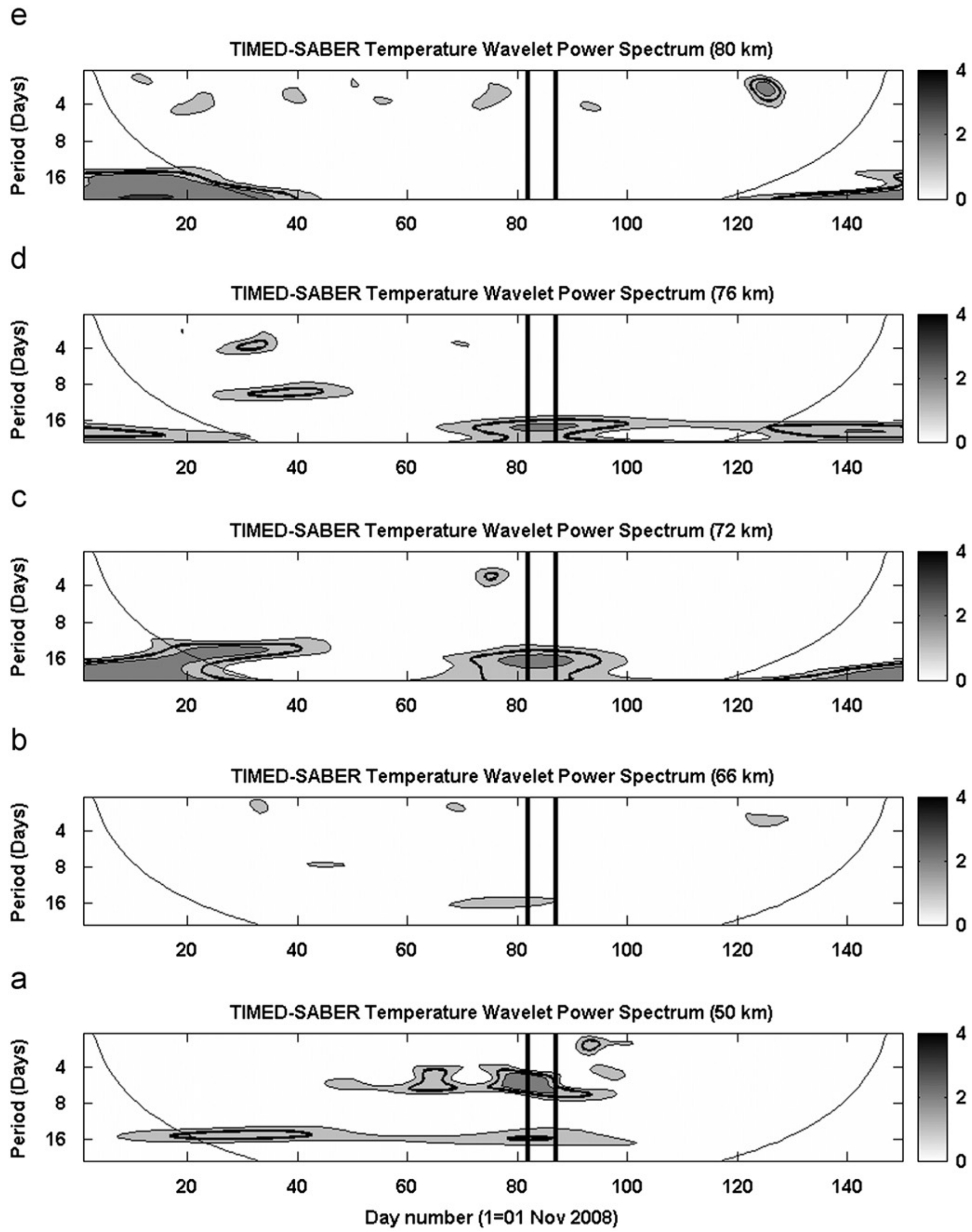

Fig. 4. (a)–(e) Wavelet (Morlet) normalized variance of TIMED-SABER temperature averaged for the longitudes 60–90°E and latitudes 10–15°N, for the altitudes 50, 66, 72, 76 and 80 km. The vertical thick bars denote the duration of the SSW event. Thick contour is the 95% confidence level.

is a major SSW event in the high latitude stratosphere. A comparison with TIMED-SABER temperature profiles confirms the warming event; however, the warmer altitude region is slightly lower than the one observed by the lidar. The potential energy per unit mass derived from the lidar temperature fluctuations, which are assumed to be due to gravity waves, shows values two times larger than that prior to the warming event.

The relationship between sudden stratospheric warming events and mesospheric temperature inversion over tropical latitudes has not yet been established. We believe that the relationship can be established through planetary waves considering the following two facts. (1) SSW is caused by anomalous growth of planetary waves in the mid- and high-latitude troposphere, which, while propagating vertically, carry poleward heat flux, leading to warming. While propagating vertically, they also refract towards tropics (Matsuno, 1971). (2) One of the causative mechanisms of mesospheric inversion layers is the planetary wave critical level interaction (Meriwether and Gerrard, 2004).

In the present study, an enhanced 16-day planetary wave activity is observed during the SSW event at altitudes 50–70 km in TIMED-SABER temperatures averaged over 10–15°N and 60–90°E, whereas the wave activity is observed to be damped at 80 km altitude. Air-glow observations also show changes in the thermal structure at mesospheric altitudes in relation to the SSW events. Walterscheid et al. (2000) observed mesospheric cooling over Eureka, a high latitude (80°N) site in Canada. Their comparative model simulation indicated alternating regions of cooling and warming above the main warming in the lower stratosphere. Our low-latitude lidar observations also show alternating cooling and warming regions. The lidar temperature averaged for nights before the warming exceeds that during

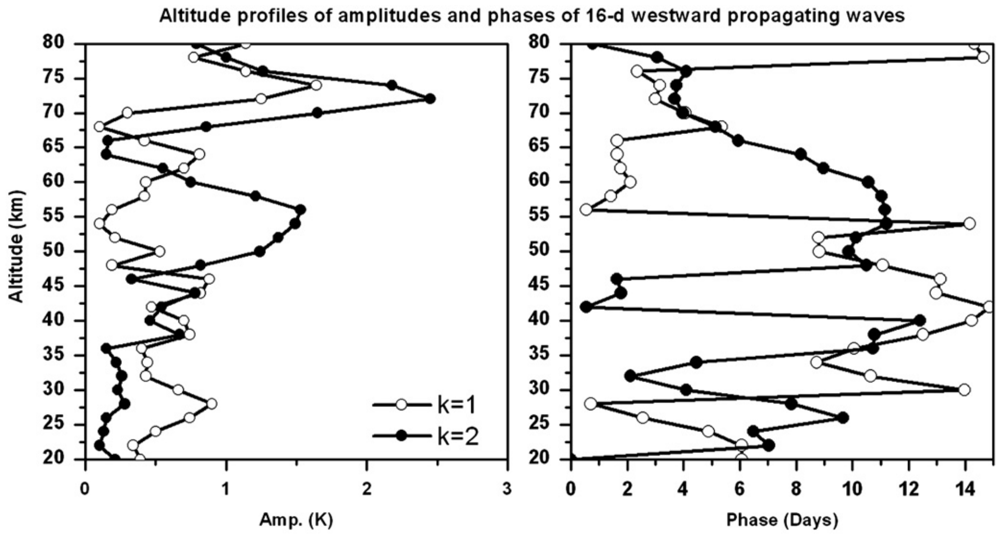

Fig. 5. Altitude profiles of amplitudes and phases of ~16-day westward propagating wave with zonal wave numbers 1 and 2.

warming by 5–7 K at altitudes 55–63 km and is lower by 10–15 K at altitudes 70–78 km. Recently Vineeth et al. (2009) noted amplified wave signatures of 16-day period during the course of an SSW event in the daytime multi-wavelength dayglow photometer measurements of the OH (8–3) airglow intensity of rotational lines at 731.6 and 740.2 nm over Trivandrum (8.5°N, 76.5°E). The authors proposed that during the SSW year, the westward propagating waves, including the quasi-16-day wave, could propagate upward through the prevailing eastward lower stratospheric circulation and get dissipated over the mesospheric region. Though eastward winds prevail during the SSW at lower stratosphere, strong westward winds of ~60 m/s develop at mesospheric altitudes and they intensify during the SSW events of 2005–2006, 2003–2004 and 1998–1999 (Sathishkumar et al., 2009). Sathishkumar and Sridharan (2009) observed reduced planetary wave activity over Tirunelveli (8.7°N, 77.8°E) during the SSW events of 1998–1999 and 2005–2006 and the reduced planetary wave activity persisted even several days after the end of the warming events. It was interpreted that the reduced planetary wave activity could be due to the presence of a critical level in the form of strong westward winds at low-latitude upper stratospheric heights due to the circulation change caused by the SSW events. Similar analysis is extended for the 2009 event also. The daily mean UKMO zonal mean temperature difference (90–60°N), zonal mean zonal wind at 60°N, zonal mean temperature at 12°N and zonal mean zonal wind at 13°N for a time interval of 1–60 days starting from 01 January 2009 are shown for pressure levels ~30 to ~0.3 hPa in Fig. 6. The onset of the SSW can again be inferred from the figure with large positive poleward temperature difference between the latitudes 90°N and 60°N on 21 January 2009 and the warming persists all through the pressure levels 30–1.5 hPa. At levels 1.5–0.3 hPa, the warming occurs a few days earlier. The warm low-latitude stratopause observed by Sridharan et al. (2009) for the 2006 event can again be observed for the 2009 event also. However, we can infer that the meridional circulation change produced by the SSW event of 2009 does not generate large westward winds, unlike other major SSW events, at low-latitude upper stratospheric altitudes and the maximum westward winds of only ~30 m/s are observed at 13°N during day numbers 30–35. The planetary wave may not have undergone critical level interaction in the presence of these weak westward winds at stratopause altitudes. Hence there could be a leakage of planetary wave flux to higher altitudes above stratopause. Though the 16-day wave could cross stratopause, it is damped at 80 km, indicating that the wave may have undergone wave damping due to large amplitudes or critical level interaction at altitudes just below 80 km and this may lead to enhanced mesospheric temperatures (Meriwether and Gerrard, 2004). Sassi et al. (2002) demonstrated that simulation of the breaking of planetary waves in the mesosphere region would produce a warming with amplitude of 10–50 K depending on strength of the planetary waves. The warming events arise as a consequence of dissipation of rapidly breaking waves that takes place when the waves encounter a critical line of zero wind.

The results presented here show that the gravity wave potential energy per unit mass increases by 2–3 times during the SSW event, when compared with the same before the event. Earlier observation and model studies were focused on wave propagation and changes in thermal structure in the high latitude winter stratosphere during SSW events. Lindzen (1981) anticipated that during SSW events, when westward winds may develop in the stratosphere, the upward propagation of quasi-stationary gravity waves would be inhibited. Whiteway and Carswell (1994) noted a cool mesosphere in their high latitude Rayleigh lidar observations and substantially greater dissipation of gravity wave energy within the upper stratospheric warming in comparison with preceding and following periods. They suggested referring to earlier model results of Lindzen (1981) and Holton (1983) and Dunkerton and Butchart (1984) that the inhibition of upward propagation of gravity waves leads to a cooling toward radiative equilibrium in the mesosphere. However, the TIME-GCM model results of Liu and Roble (2002) showed that the weakening and reversal of stratospheric jet could allow increasing amounts of eastward propagating gravity waves to penetrate into the mesospheric heights and break there. The eastward forcing due to breaking of gravity waves in the winter hemisphere induces an equatorward and upward flow at mesospheric altitudes leading to a temperature decrease of about 50 K at high latitudes. Sridharan and Sathishkumar (2008) noted increased gravity wave variance over Tirunelveli consistently during late winter of SSW years. The prevailing westward winds at stratospheric heights may have allowed eastward propagating gravity waves to reach mesospheric altitudes. The increased gravity wave variance noted earlier even several days after the SSW events over Tirunelveli (Sathishkumar and Sridharan, 2009) could not be observed here in the lidar temperatures over Gadanki, as lidar observations were

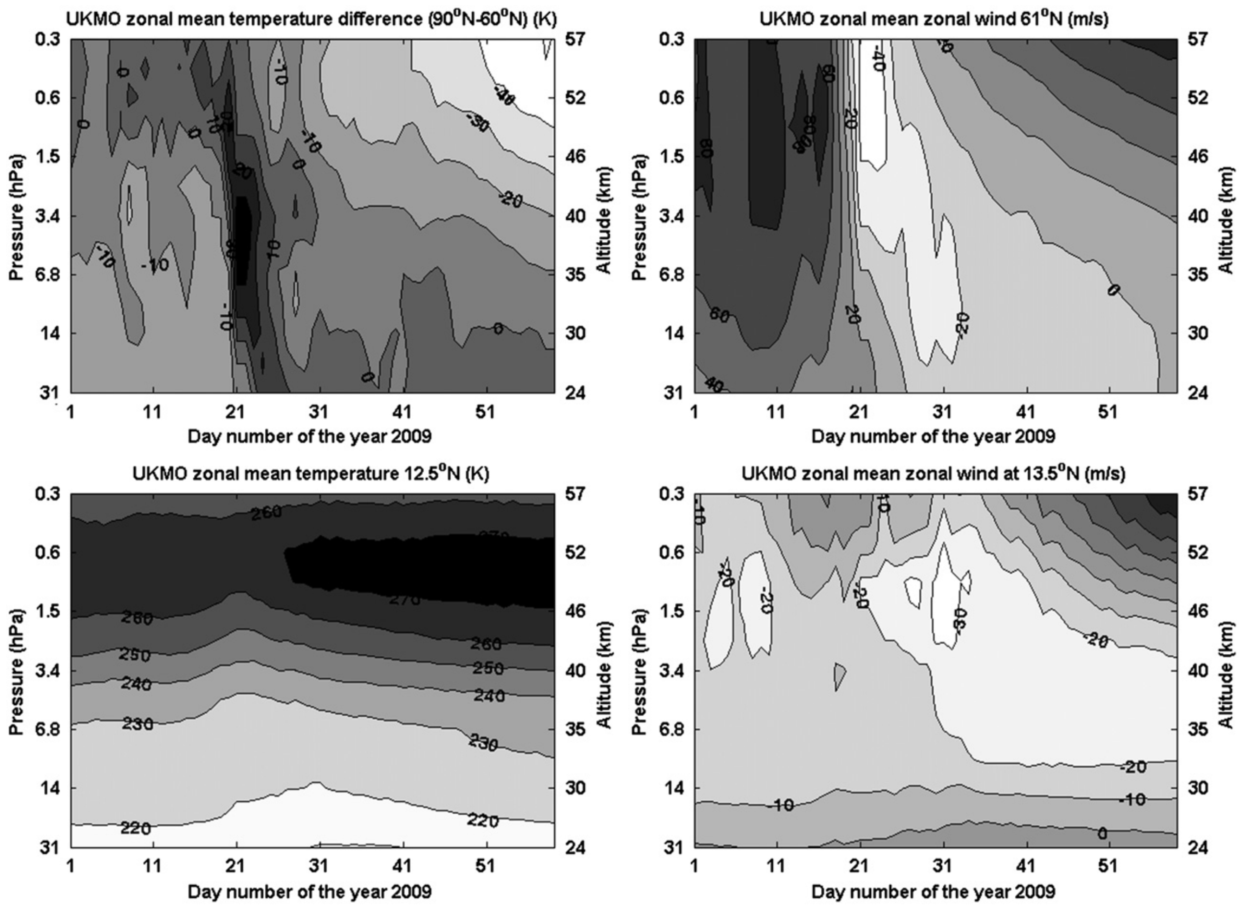

Fig. 6. Time variation of daily mean UKMO zonal mean temperature difference (90–60°N) (left top), UKMO zonal mean zonal wind at 61°N (right top), UKMO zonal mean temperature at 12.5°N (left bottom) and UKMO zonal mean zonal wind at 13.5°N (right bottom) for a time interval of 1–59 days starting from 01 January 2009.

not carried out after the SSW event due to a problem in the laser unit. In the forthcoming winters, lidar and radar experiments will be conducted simultaneously in order to understand the effect of SSW on gravity wave propagation at low latitudes prior, during and after the SSW event.

Acknowledgements

The authors would like to acknowledge the SAFAR program of NARL and the support rendered by technical staff in conducting the lidar observations. They also gratefully acknowledge the UK Meteorological Office and TIMED-SABER team for providing the data used in this study. They would like to thank the Editor and the two referees for their critical comments and suggestions, which helped them to improvise the manuscript.

References

Andrews, D.G., Holton, J.R., Leovy, C.B., 1987. Middle Atmospheric Dynamics. Elsevier, New York 489pp.

Daubechies, I., 1992. Ten Lectures on Wavelets. Society for Industrial and Applied Mathematics, University Science Centre, Philadelphia, PA 357pp.

Dunkerton, T.J., Butchart, N., 1984. Propagation and selective transmission of internal gravity waves in a sudden warming. Journal of the Atmospheric Sciences. doi:10.1175/1520-0469.

Fritz, S., Soules, S.D., 1970. Large-scale temperature changes in the stratosphere observed from Nimbus III. Journal of the Atmospheric Sciences. doi:10.1175/1520-0469.

Gregory, J.B., Manson, A.H., 1975. Winds and wave motions to 110 km at midlatitudes, III. Response of mesospheric and thermospheric winds to major stratospheric warmings. Journal of the Atmospheric Sciences. doi:10.1175/1520-0469.

Guharay, A., Nath, D., Pant, P., Pande, B., Russell III, J.M., Pandey, K., 2009. Middle atmospheric thermal structure obtained from Rayleigh lidar and TIMED/SABER observations: a comparative study. Journal of Geophysical Research 114, D18105. doi:10.1029/2009JD011963.

Hauchecorne, A., Chanin, M.L., 1980. Density and temperature profiles obtained by lidar between 35 and 70 km. Geophysical Research Letters 7, 565–568.

Holton, J.R., 1983. The influence of gravity wave breaking on the general circulation of the middle atmosphere. Journal of the Atmospheric Sciences. doi:10.1175/1520-0469.

Jayaraman, A., Venkat Ratnam, M., Patra, A.K., Narayana Rao, T., Sridharan, S., Rajeevan, M., Gadhavi, H., Kesarkar, A.P., Srinivasalu, P., Raghunath, K., 2009. Study of atmospheric forcing and responses (SAFAR) campaign: overview. Annales Geophysicae 1 (89–101), 2010.

Labitzke, K., Naujokat, B., 2000. The lower Arctic stratosphere in winter since 1952. SPARC Newsletter 15, 11–14.

Lima, L.M., Batista, P.P., Clemesha, B.R., Takahashi, H., 2006. 16-day wave observed in the meteor winds at low latitudes in the southern hemisphere. Advanced Space Science. doi:10.1016/j.asr.2006.03.033.

Lindzen, R.S., 1981. Turbulence and stress owing to gravity wave and tidal breakdown. Journal of Geophysical Research 86, 9707–9714.

Liu, H.-L., Roble, R.G., 2002. A study of a self-generated stratospheric sudden warming and its mesospheric–lower thermospheric impacts using the coupled TIME-GCM/CCM3. Journal of Geophysical Research 107 (D23), 4695. doi:10.1029/2001JD001533.

Luo, Y., Manson, A.H., Meek, C.E., Thayaparan, T., MacDougall, J., Hocking, W.K., 2002. The 16-day wave in the mesosphere and lower thermosphere: simultaneous observations at Saskatoon (52°N, 107°W) and London (43°N, 81°W), Canada. Journal of Atmospheric and Solar–Terristrial Physics 64 (8–11), 1287–1307.

Manney, G.L., Schwartz, M.J., Krüger, K., Santee, M.L., Pawson, S., Lee, J.N., Daffer, W.H., Fuller, R.A., Livesey, N.J., 2009. Aura Microwave Limb Sounder observations of dynamics and transport during the record-breaking 2009

Arctic stratospheric major warming. Geophysical Research Letters 36, L12815. doi:10.1029/2009GL038586.

Matsuno, T., 1971. A dynamical model of the stratospheric sudden warming. Journal of the Atmospheric Sciences. doi:10.1175/1520-0469.

Meriwether, J.W., Gerrard, A.J., 2004. Mesosphere inversion layers and stratosphere temperature enhancements. Review of Geophysics 42, RG3003. doi:10.1029/2003RG000133.

Mertens, C.J., et al., 2004. SABER observations of mesospheric temperatures and comparisons with falling sphere measurements taken during the 2002 summer MaCWAVE campaign. Geophysical Research Letters 31, L03105. doi:10.1029/2003GL018605.

Mukherjee, B.K., Ramana Murty, Bh.V., 1972. High-level warmings over a tropical station. Monthly Weather Review. doi:10.1175/1520-0493(1972)100.

Remsberg, E., Lingenfelser, G., Harvey, V.L., Grose, W., Russell III, J., Mlynczak, M., Gordley, L., Marshall, B.T., 2003. On the verification of the quality of SABER temperature, geopotential height, and wind fields by comparison with Met Office assimilated analyses. Journal of Geophysical Research 108 (D20), 4628. doi:10.1029/2003JD003720.

Sassi, F., Garcia, R.R., Boville, B.A., Liu, H., 2002. On temperature inversions and the mesospheric surf zone. Journal of Geophysical Research 107 (D19), 4380. doi:10.1029/2001JD001525.

Sathishkumar, S., Sridharan, S., 2009. Planetary and gravity waves in the mesosphere and lower thermosphere region over Tirunelveli (8.7°N, 77.8°E) during stratospheric warming events. Geophysical Research Letters 36, L07806. doi:10.1029/2008GL037081.

Sathishkumar, S., Sridharan, S., Jacobi, Ch., 2009. Dynamical response of low-latitude middle atmosphere to major sudden stratospheric warming events. Journal of Atmospheric and Solar–Terrestrial Physics. doi:10.1016/j.jastp.2009.04.002.

Scherhag, R., 1952. Die explosionsartige Stratosphärenerwärmung des Spätwinters 1951/52. Berichtedes Deutrehen Wetterdienstes US-Zone 6 (38), 51–63.

Shepherd, M.G., Wu, D.L., Fedulina, I.N., Gurubaran, S., Russell, J.M., Mlynczak, M.G., Shepherd, G.G., 2007. Stratospheric warming effects on the tropical mesospheric temperature field. Journal of Atmospheric and Solar–Terrestrial Physics. doi:10.1016/j.jastp.2007.04.009.

Siva Kumar, V., Rao, P.B., Krishnaiah, M., 2003. Lidar measurements of stratosphere–mesosphere thermal structure at a low latitude: comparison with satellite data and models. Journal of Geophysical Research 108 (D11), 4342. doi:10.1029/2002JD003029.

Sridharan, S., Sathishkumar, S., 2008. Seasonal and interannual variations of gravity wave activity in the low-latitude mesosphere and lower thermosphere over Tirunelveli (8.7°N, 77.8°E). Annales Geophysicae 26, 3215–3223.

Sridharan, S., Sathishkumar, S., Raghunath, K., 2009. Rayleigh lidar observations of enhanced statopause temperature over Gadanki (13.5°N, 79.2°E) during major stratospheric warming in 2006. Annales Geophysicae 27, 373–379.

Swinbank, R., O'Neill, A., 1994. A stratosphere–troposphere data assimilation system. Monthly Weather Review. doi:10.1175/1520-0493.

Torrence, C., Compo, G.P., 1999. A practical guide to wavelet analysis. Bulletin of the American Meteorological Society 79, 61–78.

Tsuda, T., Nishida, M., Rocken, C., Ware, R.H., 2000. A global morphology of gravity wave activity in the stratosphere revealed by the GPS occultation data (GPS/MET). Journal of Geophysical Research 105 (D6), 7257–7273. doi:10.1029/1999JD901005.

Vineeth, C., Pant, T.K., Kumar, K.K., Ramkumar, G., Sridharan, R., 2009. Signatures of low latitude–high latitude coupling in the tropical MLT region during sudden stratospheric warming. Geophysical Research Letters 36, L20104. doi:10.1029/2009GL040375.

Walterscheid, R.G., Sivjee, G.G., Roble, R.G., 2000. Mesospheric and lower thermospheric manifestation of a stratospheric warming event over Eureka, Canada (80°N). Geophysical Research Letters 27, 2897–2900.

Whiteway, J.A., Carswell, A.I., 1994. Rayleigh lidar observations of thermal structure and gravity wave activity in the high arctic during a stratospheric warming. Journal of the Atmospheric Sciences. doi:10.1175/1520-0469.